

See discussions, stats, and author profiles for this publication at: <https://www.researchgate.net/publication/322376617>

Adsorption characteristics of green 5-arylaminoethylene pyrimidine-2,4,6-triones on mild steel surface in acidic medium: Experimental and computational approach

Article in *Results in Physics* · March 2018

DOI: 10.1016/j.rinp.2018.01.008

CITATIONS

8

READS

412

4 authors:



Chandrabhan Verma

North West University South Africa

101 PUBLICATIONS 1,602 CITATIONS

SEE PROFILE



Lukman O. Olasunkanmi

Obafemi Awolowo University

67 PUBLICATIONS 1,283 CITATIONS

SEE PROFILE



Eno Ebenso

North West University South Africa

205 PUBLICATIONS 2,622 CITATIONS

SEE PROFILE



Mumtaz Ahmad Quraishi

Banaras Hindu University

442 PUBLICATIONS 11,740 CITATIONS

SEE PROFILE

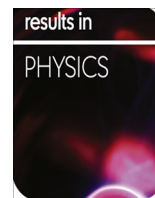
Some of the authors of this publication are also working on these related projects:



Green corrosion inhibitors [View project](#)



CORROSION SCIENCE [View project](#)



Adsorption characteristics of green 5-arylaminoethylene pyrimidine-2,4,6-triones on mild steel surface in acidic medium: Experimental and computational approach

Chandrabhan Verma^{a,b,*}, Lukman O. Olasunkanmi^{a,b,c}, Eno E. Ebenso^{a,b,*}, M.A. Quraishi^d

^a Department of Chemistry, School of Mathematical & Physical Sciences, Faculty of Agriculture, Science and Technology, North-West University (Mafikeng Campus), Private Bag X2046, Mmabatho 2735, South Africa

^b Material Science Innovation & Modelling (MaSIM) Research Focus Area, Faculty of Agriculture, Science and Technology, North-West University (Mafikeng Campus), Private Bag X2046, Mmabatho 2735, South Africa

^c Department of Chemistry, Faculty of Science, Obafemi Awolowo University, Ile-Ife 220005, Nigeria

^d Center of Research Excellence in Corrosion, Research Institute, King Fahd University of Petroleum & Minerals, Dhahran 31261, Saudi Arabia

ARTICLE INFO

Article history:

Received 7 November 2017

Received in revised form 19 December 2017

Accepted 4 January 2018

Available online 10 January 2018

Keywords:

Multicomponent reactions

Green corrosion inhibitors

Acid solution

Theoretical studies

Langmuir adsorption isotherm

ABSTRACT

The effect of electron withdrawing nitro ($-\text{NO}_2$) and electron releasing hydroxyl ($-\text{OH}$) groups on corrosion inhibition potentials of 5-arylaminoethylene pyrimidine-2,4,6-trione (AMP) had been studied. Four AMPs tagged AMP-1, AMP-2, AMP-3 and AMP-4 were studied for their ability to inhibit mild steel corrosion in 1 M HCl using experimental and theoretical methods. Gravimetric results showed that inhibition efficiency of the studied inhibitors increases with increasing concentration. The results further revealed that that electron withdrawing nitro ($-\text{NO}_2$) group decreases the inhibition efficiency of AMP, while electron donating hydroxyl ($-\text{OH}$) group increases the inhibition efficiency of AMP. SEM and AFM studies showed that the studied compounds inhibit mild steel corrosion by adsorbing at the metal/electrolyte interface and their adsorption obeyed the Temkin adsorption isotherm. Potentiodynamic polarization study revealed that studied inhibitors act as mixed type inhibitors with predominant effect on cathodic reaction. The inhibitive strength of the compounds might have direct relationship electron donating ability of the molecules as revealed by quantum chemical parameters. The order of interaction energies derived from Monte Carlo simulations is $\text{AMP-4} > \text{AMP-3} > \text{AMP-2} > \text{AMP-1}$, which is in agreement with the order of inhibition efficiencies obtained from experimental measurements.

© 2018 The Authors. Published by Elsevier B.V. This is an open access article under the CC BY license (<http://creativecommons.org/licenses/by/4.0/>).

Introduction

Acid solutions are commonly used in many industries for various purposes such as acid cleaning, acid descaling, oil well cleaning, acid pickling etc [1,2]. However, these industrial processes are accompanied by corrosive dissolution of metals in the acid solutions [2–5]. Several methods have been described in literature for the protection of metals against corrosion in acid solution. The use of organic molecules containing heteroatoms particularly, N, O and S as corrosion inhibitors is one of the most economic, popular and practical methods of strangling corrosion rate [6–9]. Inhibition of metal corrosion by organic molecules has been widely described

as a function of the degree of adsorption of the inhibitor molecules on metallic surface. Therefore investigation of inhibitor adsorption at metal/electrolyte interface is an important topic in corrosion studies [7,8,10].

Previous studies have revealed that the adsorption of organic inhibitor molecules on metallic surface mainly depends on physicochemical properties such as the nature of functional groups, chemical and electronic structure, solution temperature, electron density at donor atoms, molecular size as well pi-orbital character of the inhibitor molecule in addition to the nature of electrolyte and the metal/alloy being investigated [8–10]. Barbituric acid and its derivatives have been extensively used for synthesis of compounds having several biological activities such as antibacterial, antihypertensive and so on [11–17]. Since, molecules derived from barbituric acids possess several heteroatoms, polar functional groups and pi-bonds and aromatic rings, corrosion inhibition potentials of barbituric acid derivatives have been extensively studied [18–20].

* Corresponding authors at: Department of Chemistry, School of Mathematical & Physical Sciences, Faculty of Agriculture, Science and Technology, North-West University (Mafikeng Campus), Private Bag X2046, Mmabatho 2735, South Africa.

E-mail addresses: chandrabhan.rs.apc@itbhu.ac.in (C. Verma), Eno.Ebenso@nwu.ac.za (E.E. Ebenso).

Considering the continuous strictness of environmental regulations and increasing ecological awareness, recent researches in all fields of science including corrosion are being directed towards “green” science [21–24]. Multicomponent reactions (MCRs), which combine three or more starting materials (MCRs) in a one-step process have emerged as a potential “green” and sustainable method for the synthesis of variety of organic compounds, particularly biochemically active heterocyclics [25,26]. MCRs are characterized by minimum waste product due to very limited workups, facile automation, simple purification, high chemical selectivity, mild reaction condition, shorter reaction time, high yield, atom economy and ease of operation. These characteristics increase the synthetic efficiency and other green aspects of the multicomponent reactions [27,28]. The use of organic solvents as reaction media in conventional synthesis is often associated with several problems, most of which are due to the toxic nature, hazardous effect, flammability and high cost of the solvent [29–31]. In this regards, the use of water as a reaction medium for organic synthesis has attracted substantial attention because it is free and readily available, it is cheap, non-toxic, non-flammable, non-hazardous and inexpensive. Water also possesses unique redox stability, and it is environmental friendly [32–34].

In view of this, the present study investigated the corrosion inhibition efficiency of four 5-arylamino-methylene-pyrimidine-2,4,6-trione (AMPs) namely, 5-(((4-nitrophenyl)amino)methylene)pyrimidine-2,4,6-(1H,3H,5H)-trione (AMP-1), 5-((phenylamino)methylene)pyrimidine-2,4,6-(1H,3H,5H)-trione (AMP-2), 5-(((4-hydroxyphenyl)amino)methylene)pyrimidine-2,4,6-(1H,3H,5H)-trione (AMP-3) and 5-(((2,4-dihydroxyphenyl)amino)methylene)pyrimidine-2,4,6-(1H,3H,5H)-trione (AMP-4), which were synthesized via three component one step reaction technique in water. The corrosion inhibition tests were carried out on mild steel in 1 M HCl using gravimetric, electrochemical impedance spectroscopy (EIS), potentiodynamic polarization, scanning electron microscopy (SEM), atomic force microscopy (AFM). Theoretical quantum chemical calculation and Monte Carlo simulations studies were carried out to corroborate experimental studies. Electron donating (–OH) substituent was found to enhance the inhibition efficiency of AMP, while electron withdrawing (–NO₂) substituent reduced the inhibition efficiency.

Experimental

Materials

Electrodes and reagents

Mild steel specimen of chemical compositions (%wt): C (0.076), Mn (0.192), P (0.012), Si (0.026), Cr (0.050), Al (0.023), and balanced with Fe was used as test material for all weight loss and electrochemical experiments. Before starting the experiments, exposed surface area of the specimens were abraded with SiC emery papers of 600, 800, 1000 and 1200 grit sizes, cleaned with double distilled

water, degreased with acetone, and finally ultrasonically cleaned with absolute ethanol. Test solution of 1 M HCl was prepared from 30% hydrochloric acid purchased from MERCK India LTD and double deionized water.

Synthesis of 5-arylamino-methylene pyrimidine 2, 4, 6-trione (AMPs)

The AMPs used as corrosion inhibitors in the present study were synthesized by method reported in literature and schematized as shown in Fig. 1 [35]. In a typical procedure, a mixture of aniline and its derivatives (1 mmol), formic acid (4 mmol), barbituric acid (1 mmol) and distilled water (5 mL) were refluxed in round bottom flask (10 mL) at 60 °C for 2–3 h. The progress and completion of the reaction was determined by TLC method. The IUPAC name, chemical structures, molecular formulas, and analytical data of the synthesized 5-arylamino-methylene pyrimidine 2, 4, 6-trione (AMPs) are given in Table 1.

Corrosion tests

Gravimetric measurements

Mild steel with the previously stated chemical compositions was cut into 2.5 cm × 2.5 × 0.025 cm dimension and used for all gravimetric measurements. The specimens were dipped into 1 M HCl for 3 h in the absence and presence of different concentrations of the synthesized corrosion inhibitors. Triplicate measurements were performed both in the absence and presence of the inhibitors, and the mean value was reported in each case. The evaluated weight loss (in mg) was used to calculate the corrosion inhibition efficiency (%) using the equation [36,37]:

$$\eta\% = \frac{w_0 - w_i}{w_0} \times 100 \quad (1)$$

where w_0 and w_i are the weight loss values in the absence and presence of different concentrations of AMPs, respectively.

Electrochemical measurements

Gamry Potentiostat/Galvanostat (Model G-300) pre-installed with Gamry Echem Analyst 5.0 software was used for all electrochemical analyses. The experimental setup comprises a three-electrode system with mild steel as working electrode, platinum foil as auxiliary or counter electrode and saturated calomel electrode (SCE) as reference electrode. The working electrode was fabricated to have an exposed surface area of 1 cm² (rest part of the specimens was covered with epoxy resin). The working electrode was immersed in 1 M HCl in the absence and presence of different concentrations of AMPs and left unperturbed for 30 min to attain a stable open circuit potential (OCP). Potentiodynamic polarization curves (anodic and cathodic) were plotted by automatically changing the electrode potential from –0.25 V to +0.25 V with respect to the stable OCP. Extrapolation of linear segments of anodic and cathodic Tafel slopes led to the evaluation of corrosion current

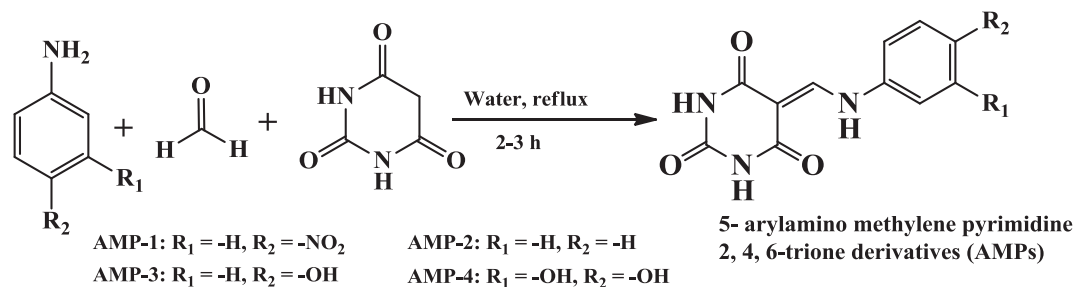


Fig. 1. General scheme for the synthesis of 5-arylamino-methylene pyrimidine 2, 4, 6-triones (AMPs).

Table 1
IUPAC name, molecular structure, molecular formula, melting point and analytical data for the synthesized AMPs.

S. No.	IUPAC name and abbreviation of Inhibitor	Chemical Structure	Molecular formula and M.P. and analytical data
1	5-(((4-nitrophenyl)amino)methylene)pyrimidine-2,4,6(1H,3H,5H)-trione (AMP-1)		Mol. formula: C ₁₁ N ₈ N ₄ O ₅ ; Mol. Wt. 276.21; FT-IR (KBr, cm ⁻²): 3563, 3442, 2978, 2857, 2398, 1725, 1660, 1268, 1223, 1148, 989, 826, 735, 652, 627; 1H NMR (500 MHz, DMSO-d/TMS) δ ppm: 11.18, 8.83, 7.63–7.92, 6.97, 5.21.
2	5-((phenylamino)methylene)pyrimidine-2,4,6(1H,3H,5H)-trione (AMP-2)		Mol. formula: C ₁₁ N ₉ N ₃ O ₃ ; Mol. Wt. 231.21; FT-IR (KBr, cm ⁻²): 3545, 3324, 2958, 2863, 2432, 1730, 1658, 1248, 1188, 972, 786, 738, 645, 614; 1H NMR (500 MHz, DMSO-d/TMS) δ ppm: 10.92, 8.56, 7.45–7.72, 6.76, 4.63.
3	5-(((4-hydroxyphenyl)amino)methylene)pyrimidine-2,4,6(1H,3H,5H)-trione (AMP-3)		Mol. formula: C ₁₁ N ₉ N ₃ O ₄ ; Mol. Wt. 247.21; FT-IR (KBr, cm ⁻²): 3360, 3622, 3574, 3388, 2954, 2865, 1709, 1640, 1239, 1212, 1128, 966, 823, 707, 632; 1H NMR (500 MHz, DMSO-d/TMS) δ ppm: 10.63, 8.78, 7.38–7.47, 6.83, 4.79, 4.32.
4	5-(((2,4-dihydroxyphenyl) amino)methylene)pyrimidine-2,4,6(1H,3H,5H)-trione (AMP-4)		Mol. formula: C ₁₁ N ₉ N ₃ O ₅ ; Mol. Wt. 263.05; FT-IR (KBr, cm ⁻²): 3656, 3640, 3418, 3364, 2934, 2884, 1713, 1648, 1232, 1193, 1124, 1072, 983, 756, 648 621; 1H NMR (500 MHz, DMSO-d/TMS) δ ppm: 9.68, 8.58, 7.24–7.39, 7.12, 6.74, 4.82, 4.17.

densities, which were used to estimate the percentage of inhibition efficiency of the inhibitors according to the equation [36,37]:

$$\eta\% = \frac{i_{\text{corr}}^0 - i_{\text{corr}}^i}{i_{\text{corr}}^0} \times 100 \quad (2)$$

where, i_{corr}^0 and i_{corr}^i are corrosion current densities in the absence and presence of AMPs, respectively.

Electrochemical impedance spectroscopic (EIS) measurements were performed for mild steel in 1 M HCl in the absence and presence of different concentrations of the studied inhibitors. The EIS measurements were recorded in the frequency range of 100 kHz to 0.01 Hz using AC signal with 10 mV amplitude (peak to peak). The values of charge transfer resistances (R_{ct}) were derived from the recorded Nyquist plots, and the corrosion inhibition efficiency was calculated using from the equation [36,37]:

$$\eta\% = \frac{R_{\text{ct}}^i - R_{\text{ct}}^0}{R_{\text{ct}}^i} \times 100 \quad (3)$$

where, R_{ct}^0 and R_{ct}^i are charge transfer resistances in the absence and presence of AMPs, respectively.

SEM and AFM measurements

Scanning electron microscopy (SEM) and atomic force microscopy (AFM) studies were performed in order to support the assertions derived from weight loss and electrochemical studies, that the AMP molecules inhibit mild steel dissolution by adsorbing onto the steel surface. For surface studies using SEM and AFM, the cleaned mild steel specimens were immersed in the test solution (1 M HCl) for 3 h in the absence and presence of optimum concentration of the inhibitor molecules. After the immersion time elapsed, the specimens were taken out, washed with water and dried using hot air blower. The steel surface was examined using SEM and AFM equipment at reasonably high resolution. For SEM analysis, Zeiss Evo 50 XVP SEM modal was used to study the surface morphology at 500x magnification. NT-MDT multimode, Russia 111 controlled by solver scanning probe microscope controller was used for AFM surface analysis. The single beam cantilever having resonance frequency in the range of 240–255 kHz in semi contact mode with corresponding spring constant of 11.5 N/m with

NOVA programme was used for image interpretation. The scanning area during AFM analysis was 10 mm × 10 mm.

Theoretical studies

Quantum chemical calculations

Molecular structures of AMPs were modeled with GaussView 5.0 software. Full geometry optimizations were carried out in the gas phase with the aid of Gaussian 09 software suite [38]. Density functional theory (DFT) method was adopted for the geometry optimizations by utilizing the B3LYP functional [39–41] together with 6–31 + G(d,p) basis set. Absence of imaginary frequency in the force constant calculations of the optimized structures confirmed that they are true energy minima. Graphical images of the optimized structures and electron density isosurfaces of the frontier molecular orbitals (FMOs) were visualized with the aid of GaussView 5.0 software. Selected quantum chemical parameters including the energy of the highest occupied molecular orbital (E_{HOMO}), energy of the lowest unoccupied molecular orbital (E_{LUMO}), the energy gap, ΔE ($\Delta E = E_{\text{LUMO}} - E_{\text{HOMO}}$), and other derived parameters were obtained. Global electronegativity (χ) and the fraction of electrons (ΔN), transferable from the inhibitor to the metal atom are among the quantum chemical descriptors that are often used to correlate corrosion inhibition strength of organic compounds. Both χ and ΔN respectively were computed according to the equations [42–44]:

$$\chi = -\frac{1}{2}(E_{\text{LUMO}} + E_{\text{HOMO}}) \quad (4)$$

$$\Delta N = \frac{\chi_{\text{Fe}} - \chi_{\text{inh}}}{2(\eta_{\text{Fe}} + \eta_{\text{inh}})} \quad (5)$$

where χ_i and η_i ($i = \text{Fe}$ or inh) are the electronegativity and hardness respectively of atomic iron (Fe) and inhibitor molecule. Hardness of bulk Fe was approximated as 0 eV/mol, while work function (ϕ) of atomic Fe was taken as 4.52 eV/mol [6]. Recently, use of work function (ϕ) for calculation of ΔN values is more common and frequent as compared to the electronegativity of the iron (Fe). The reported values of work functions of iron for Fe(1 0 0), Fe(1 1 0) and Fe(1 1 1) are 4.64 eV, 4.52 eV and 4.74 eV, respectively. Owing to the asso-

Table 2
Weight loss parameters obtained for mild steel in 1 M HCl containing different concentrations of AMPs.

Inhibitors	Conc (mM)	Weight loss (mg)	C_R ($\text{mg cm}^{-2}\text{h}^{-1}$)	Inhibition efficiency ($\eta\%$)	Surface coverage (θ)
Blank	–	230	7.66	–	–
AMP-1	0.090	108	3.60	53.04	0.5304
	0.181	70	2.33	69.56	0.6956
	0.272	46	1.53	80.00	0.8000
	0.362	24	0.80	89.56	0.8956
AMP-2	0.090	101	3.36	56.08	0.5608
	0.181	63	2.10	72.60	0.7260
	0.272	39	1.30	83.04	0.8304
	0.362	19	0.63	91.73	0.9173
AMP-3	0.090	96	3.20	58.26	0.5826
	0.181	58	1.93	74.78	0.7478
	0.272	32	1.06	86.08	0.8608
	0.362	14	0.46	93.91	0.9391
AMP-4	0.090	89	2.96	61.30	0.6130
	0.181	49	1.63	78.69	0.7869
	0.272	26	0.86	88.69	0.8869
	0.362	7	0.23	96.95	0.9695

Table 3
Variation of C_R and $\eta\%$ with temperature for mild steel corrosion in 1 M HCl in the absence and presence of optimum concentration of AMPs.

Temperature (K)	Corrosion rate (C_R) ($\text{mg cm}^{-2}\text{h}^{-1}$) and Inhibition efficiency ($\eta\%$)									
	Blank		AMP-1		AMP-2		AMP-3		AMP-4	
	C_R	$\eta\%$	C_R	$\eta\%$	C_R	$\eta\%$	C_R	$\eta\%$	C_R	$\eta\%$
308	7.66	–	0.80	89.56	0.63	91.73	0.46	93.91	0.23	96.95
318	11.0	–	1.86	83.03	1.56	85.75	1.26	88.48	0.76	93.03
328	14.3	–	3.93	72.55	3.63	74.65	3.13	78.13	2.16	84.88
338	18.6	–	7.73	58.57	7.13	61.78	6.6	64.64	5.50	70.53

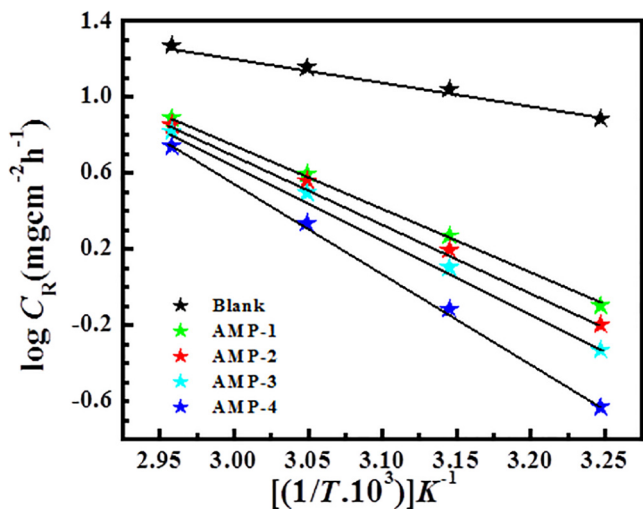


Fig. 2. Arrhenius plots for the corrosion of mild steel in 1 M HCl in the presence of different concentrations of AMPs.

ciation with minimum energy and maximum stability, the work function value of iron 4.52 eV was selected for the calculation of the fraction of electron transfer of four studied AMP molecules.

Promising local sites of reactivity on INH molecules were investigated by computing the Fukui indices, f^+ and f^- as pointers to the prospective sites of electrophilic and nucleophilic attacks respectively [42,43,45–48]. The Fukui functions were calculated using the finite difference (FD) approximation approach as [48]:

$$f_k^+ = \rho_{k(N+1)}(r) - \rho_{k(N)}(r) \quad (6)$$

$$f_k^- = \rho_{k(N)}(r) - \rho_{k(N-1)}(r) \quad (7)$$

where $\rho_{k(N+1)}$, $\rho_{k(N)}$ and $\rho_{k(N-1)}$ are the electron densities for atom k in $(N+1)$ -, (N) - and $(N-1)$ -electron systems respectively. The electron densities were approximated as Mulliken gross charges on each atom. Numerical values of f_k^+ and f_k^- were visualized as graphical electron density isosurfaces with the aid of the Multiwfn software [49,50].

Monte Carlo simulations

Fully optimized structures of AMPs were used in simulating the adsorption of AMP molecules on Fe(110) crystal surface. The cleaved Fe(110) plane was firstly optimized with COMPASS force field and then expanded into a 10×10 supercell. The surface atoms of the 10×10 supercell of the clean Fe(110) crystal was selected as the target for direct interactions with AMP molecule in each case. Adsorption locator module was used to place the adsorbent on Fe(110) surface. The simulated annealing process went through 10 cycles at 100,000 steps per cycle under ultra-fine convergence criteria.

Results and discussion

Gravimetric measurements

Effect of inhibitors concentration

Table 2 contains the weight loss parameters and corrosion inhibition efficiency and in the absence and presence of different concentrations of AMPs. The results (Table 2) showed that inhibition efficiency for all the inhibitors increases with increasing concentration and maximum efficiencies of 89.56% for AMP-1, 91.73% for AMP-2, 93.91% for AMP-3 and 96.95% for AMP-4 were obtained

at 0.362 mM and 303 K. The observed trend of inhibition efficiencies can be explained in relation to the electron withdrawing and electron donating substituents presence at the 3- (meta) and 4- (para) positions of arylamino ring. Just like our previous reports [37,51–56], the nitro ($-\text{NO}_2$) substituted 5-arylamino-methylene pyrimidine 2, 4, 6-trione (AMP-1) exhibited lower inhibition efficiency than the unsubstituted 5-arylamino-methylene pyrimidine 2, 4, 6-trione (AMP-2), which could be as a result of electron withdrawing effect of nitro ($-\text{NO}_2$) group which decreases the electron density available at the adsorption site of AMP-1, thereby decreases its inhibition efficiency. Likewise, the higher inhibition efficiency of AMP-3 compared to AMP-2 can be attributed to the presence of electron donating hydroxyl ($-\text{OH}$) group (at the 4-

(para) position) on the arylamino ring. AMP-4 has two units of electron donating ($-\text{OH}$) substituent in its molecule, i.e. at both 3- (meta) and 4- (para) positions on the arylamino ring, which synergistically increased the electron density at adsorption sites on the molecule, thereby enhanced its adsorption tendency and hence increased its corrosion inhibition efficiency.

Effect of temperature

Variation of inhibition efficiencies and corrosion rates with temperature are presented in Table 3. From the results shown in Table 3, it can be seen that inhibition efficiency decreases and corrosion rate increases with increasing solution temperature from 308 to 338 K. The increased corrosion rates and decreased inhibition efficiencies upon increase in temperature is attributed to increased kinetic energy of the inhibitor molecules, which decreases attraction force between inhibitor molecules and metallic surface [57–59]. Moreover, rapid etching, molecular decomposition and molecular rearrangements may also decrease the inhibition efficiency of inhibitor molecules at elevated temperature. Arrhenius equation can be used to explain the effect of temperature on the corrosion rate (C_R), according to which the log of corrosion rate (C_R) is a linear function of $1/T$ [60,61]:

$$\log(C_R) = \frac{-E_a}{2.303RT} + \log A \quad (8)$$

where C_R is the corrosion rate in $\text{mg cm}^{-2}\text{h}^{-1}$, A is the Arrhenius pre-exponential factor, R is the gas constant and T is the absolute temperature. Straight lines were obtained for Arrhenius plots in the absence and presence of the inhibitors and the profiles are shown in Fig. 2. The values of E_a were 65.45, 70.28, 76.67, and 91.18 kJmol^{-1} for AMP-1, AMP-2, AMP-3 and AMP-4, respectively (Table S1). The values of E_a derived from Arrhenius plots for inhibited metal corrosion were much higher as compare to the value of E_a for uninhibited metallic corrosion (28.48 kJmol^{-1}). The higher values of E_a for inhibited metal corrosion as compared to the uninhibited one can be attributed to the formation of energy barrier for metallic dissolution process in the presence of inhibitor molecules [52,62,63]. Furthermore, it has been earlier reported that electrostatic interactions between charged inhibitor molecules and metallic surface might increase the value of E_a in presence of inhibitor molecules [52,62,64].

Adsorption isotherm and thermodynamic parameters

Adsorption isotherm is the most important topics in the field of corrosion because it provides some fundamental information about interactions between adsorbate (inhibitor) and adsorbent (metallic surface). Depending on the electronic structure of inhibitor molecule, nature of metal and electrolyte, solution temperature, etc. adsorption may be chemisorption, physisorption or both. In this study, several commonly used isotherms namely; Langmuir, Temkin, Frumkin and Freundlich were tested among which Temkin adsorption isotherm gave the best line of fit, with the values of regression coefficient (R^2) very close to unity for all the inhibitors. The values of the slopes, intercepts, and regression coefficients for Langmuir and Temkin adsorption isotherms are

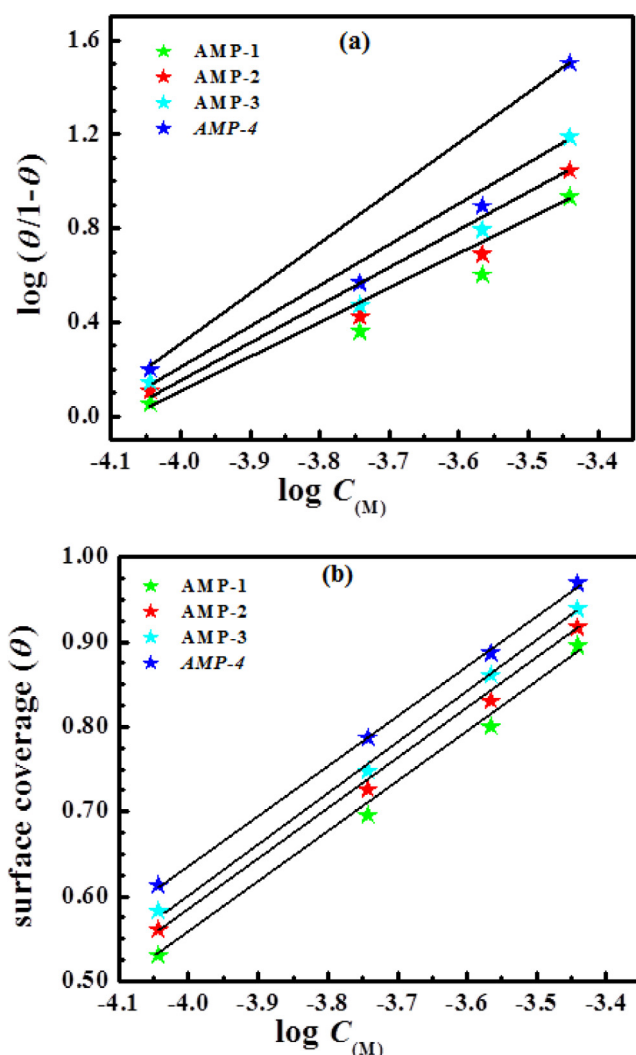


Fig. 3. (a) Langmuir, and (b) Temkin adsorption isotherm plots for the adsorption of AMPs on mild steel surface in 1 M HCl.

Table 4

K_{ads} and $\Delta G^{\circ}_{\text{ads}}$ for mild steel in 1 M HCl in the absence and presence of optimum concentration of AMPs at different temperatures (data derived from Temkin adsorption isotherms).

Inhibitor	K_{ads} (10^4 M^{-1})				$-\Delta G^{\circ}_{\text{ads}}$ (kJmol^{-1})			
	308	318	328	338	308	318	328	338
AMP-1	1.03	0.58	0.31	0.16	33.95	33.57	32.94	32.19
AMP-2	1.33	0.72	0.35	0.19	34.61	34.12	33.24	32.57
AMP-3	1.85	0.92	0.42	0.21	35.45	34.76	33.77	32.91
AMP-4	3.81	1.60	0.67	0.28	37.31	36.22	35.00	33.67

presented in Table S2 of the Supporting Information. The Langmuir and Temkin adsorption isotherms are given in Fig. 3. The Temkin isotherm can be described by the equation [65]:

$$\exp(-2a\theta) = K_{\text{ads}} C_{(\text{inh})} \quad (9)$$

where, θ is the surface coverage, $C_{(\text{inh})}$ is the inhibitor concentration, K_{ads} is the equilibrium constant for adsorption–desorption processes and 'a' is the molecular interaction parameters. The value of Gibb's free energy (ΔG_{ads}^0) of adsorption for the inhibitor molecules on metallic surface was calculated from the equation:

$$\Delta G_{\text{ads}}^0 = -RT \ln(55.5K_{\text{ads}}) \quad (10)$$

where, R is the universal gas constant, T is the absolute temperature (K), while the numerical value of 55.5 represents the concentration of water in aqueous acid solution. The calculated values of free energy of adsorption (ΔG_{ads}^0) and equilibrium constant (K_{ads}) are presented in Table 4.

High values of K_{ads} and negative values of ΔG_{ads}^0 were obtained for the studied inhibitors over the studied temperature range, indicating that the inhibitor molecules adsorb spontaneously on the mild steel surface by strong intermolecular force of attraction [66]. Furthermore, literature survey reveals that value of ΔG_{ads}^0 are frequently used to describe the nature of adsorption. In general, adsorption of an inhibitor with large negative value of ΔG_{ads}^0 (-40 kJmol^{-1} or more negative) is associated with charge transfer between inhibitor and metal (chemisorption), while one with lower negative value of ΔG_{ads}^0 (-20 kJmol^{-1} or less negative) might involve electrostatic interaction (physisorption) between charged inhibitor molecules and metallic surface [67,68]. In the present study, the values of ΔG_{ads}^0

vary from 32.19 to 37.31 kJmol^{-1} , suggesting that the interactions between inhibitor molecules and metallic surface are might involve combination of both physisorption and chemisorption mechanisms [69,70].

Electrochemical measurements

Potentiodynamic polarization measurements

Potentiodynamic polarization curves for mild steel working electrode in 1 M HCl solution without and with optimum concentrations of the inhibitor molecules are shown in Fig. 4. The polarization parameters derived from the measurements and corresponding inhibition efficiencies are presented in Table 5. It can be seen that corrosion current density (i_{corr}) decreases significantly in the presence of the inhibitors, suggesting that the studied compounds (AMPs) inhibit mild steel corrosion in 1 M HCl solution. It has been reported that the shift in the value of corrosion potential (E_{corr}) is an important parameter for adjudging whether the inhibitive effect is cathodic or anodic biased. In general, when the shift in the value of E_{corr} in presence of the inhibitor with respect to the E_{corr} for the blank is less than 85 mV, the inhibitor is considered to affect both the anodic metallic dissolution and cathodic hydrogen evolution [71,72]. That is, the compound acts as a mixed-type inhibitor. In the present study, the maximum shift in the E_{corr} value in presence of inhibitor molecules with respect to the E_{corr} of the blank, were 72, 79, 76 and 75 mV for AMP-1, AMP-2, AMP-3 and AMP-4, respectively suggesting that all studied inhibitor molecules behave as mixed type inhibitors [71,72]. However, careful examination of the results shown in Table 5 revealed that in the presence of the inhibitors the values of cathodic slopes are comparatively more affected, especially for AMP-1 and AMP-2, suggesting that although the studied inhibitors inhibit both cathodic and anodic reactions, their effects on the cathodic reactions are comparatively greater [52,53,71,72].

Electrochemical impedance spectroscopic (EIS) measurements

EIS studies have been extensively used as an excellent technique in understanding the mechanism of electrochemical reactions such as corrosion, passivation, and charge transfer reactions occurring on metal/electrolyte interface. Fig. 5a represents the Nyquist plots for inhibited and uninhibited mild steel corrosion in 1 M HCl. It can be seen that the shape of Nyquist plots for inhibited and uninhibited specimens are similar, suggesting that the studied compounds inhibit mild steel corrosion without changing the mechanism of corrosion. The Nyquist plots show a single semi-circle loop for all studied compounds over the studied frequency range, which is confirmed by single maxima in the Bode plots both in the absence and presence of inhibitors as shown in Fig. 5c.

The diameter of the Nyquist plots in the presence of the inhibitors was much high compared to that without the inhibitor. This could be as a result of adsorption and formation of protective film by the studied molecules on mild steel surface, thereby acting as barrier to corrosion process [73,74]. The equivalent circuit used for the fitting of the EIS results is shown in Fig. 5b. For metallic dissolution, replacement of the capacitance in the circuit with con-

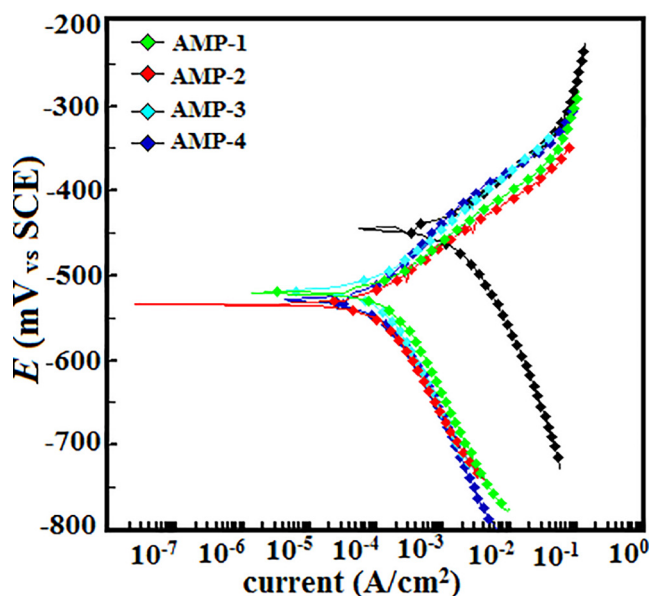


Fig. 4. Potentiodynamic polarization curves for mild steel in the absence and presence of optimum concentrations of the studied inhibitors (AMPs).

Table 5

Tafel polarization parameters for mild steel in 1 M HCl in the absence and presence of optimum concentration of AMPs.

Inhibitor	Concentration mM	E_{corr}	β_a	$-\beta_c$	i_{corr}	$\eta\%$
Blank	–	–445	70.5	114.6	1150	–
AMP-1	0.362	–517	78.3	150.5	136.0	88.17
AMP-2	0.362	–524	78.4	153.1	109.0	90.52
AMP-3	0.362	–520	72.1	129.1	87.0	92.43
AMP-4	0.362	–521	78.1	118.6	47.0	95.91

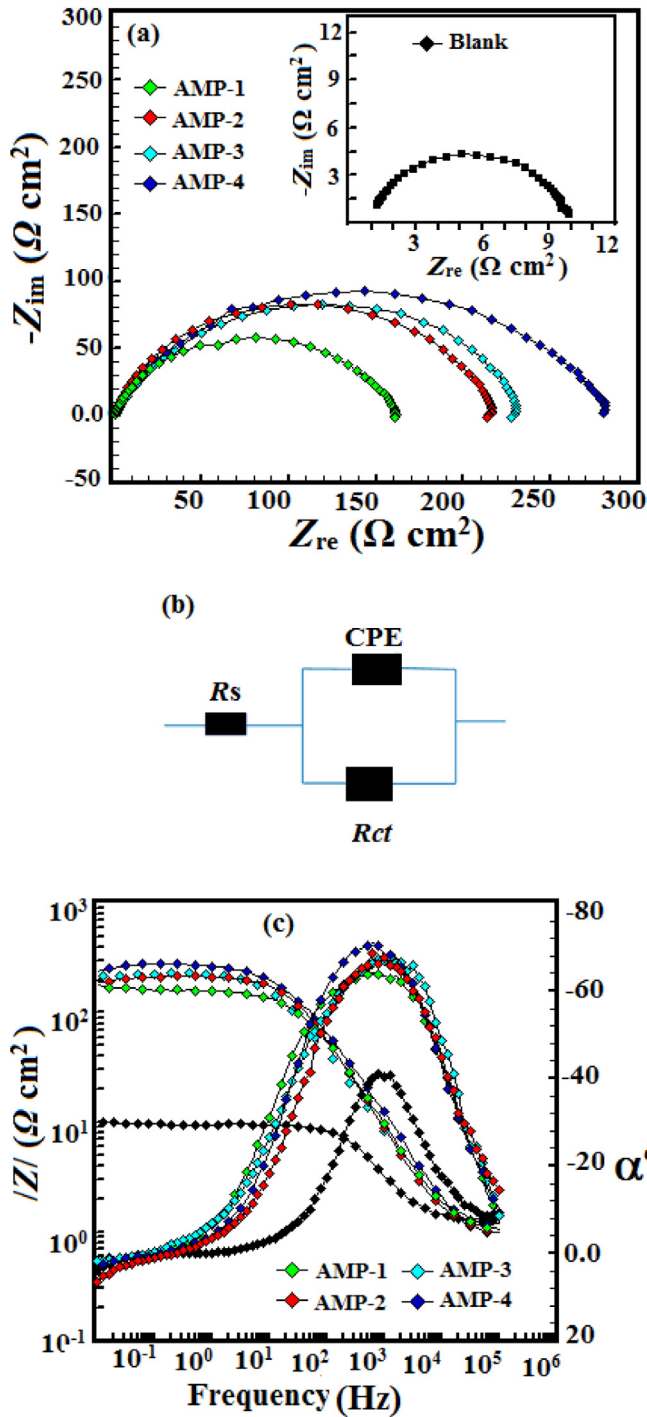


Fig. 5. (a) Nyquist plot for mild steel in 1 M HCl in the absence and presence of optimum of concentrations of AMPs, (b) Equivalent circuit used for the analysis of the EIS spectra, (c) Bode plots for mild steel in 1 M HCl in the absence and presence of optimum of concentrations of AMPs.

stant phase element (CPE) gives comparatively better approximation. The impedance CPE can be expressed as:

$$Z_{CPE} = \left(\frac{1}{Y_0}\right) [(j\omega)_n]^{-1} \tag{11}$$

where, ω is the angular frequency, j is the imaginary number, Y_0 is the CPE constant and n is the phase shift (or CPE exponent). The EIS parameters obtained from the fitting of EIS spectra using the equivalent circuit of Fig. 5b are shown in Table 6. The value of phase shift is generally related to the nature of CPE and surface inhomogeneity. A high value of phase shift (n) is associated with low surface roughness.

The results in Table 6 showed that the values of n are comparatively higher in the presence of inhibitor molecules compared to the blank, which could be as a result of increased surface smoothness due to the formation of protective film by inhibitors on the steel surface [52,53,75]. In addition, the increased phase angle of the Bode plots in the presence of inhibitors also supported the assumption that the inhibitors form protective surface film on the steel surface, which isolates the metal from corrosion environment and thereby increases surface smoothness [52,53,75]. For ideal capacitor, the values of the slope of the linear segment of $|Z|$ vs frequency plots and the phase angle should be -1 and -90° , respectively. However, the estimated values for the presented study suggested that the steel in 1 M HCl in the absence and presence of the studied inhibitors deviated from ideal capacitive behavior. This deviation is generally attributed to roughness of surface of the working electrode, which is caused by destructive corrosion of the metallic surface. However, it can also be seen that values of phase angle significantly increased in the presence of inhibitors, which further suggests that surface smoothness has been increased as a result of formation of protective film by inhibitors [52,53,75].

The CPE can represent resistance, capacitance, inductance and Warburg impedance depending on the value of n , such that is $n = 0$ ($Y_0 = R$, resistance) $n = 1$ ($Y_0 = C$, capacitance), $n = 1$ ($Y_0 = L$, inductance), and $n = 0.5$ ($Y_0 = W$, Warburg impedance) respectively. In the present study, the values of n were close to unity (0.827–0.886), suggesting that the CPE behaves closely like a capacitance. Double layer capacitance (C_{dl}) was evaluated for mild steel/electrolyte interface in the absence and presence of optimum concentration of the inhibitor molecules according to the equation [3]:

$$C_{dl} = Y_0 (\omega_{max})^{n-1} \tag{12}$$

where, ω_{max} is the frequency at which the imaginary part of impedance has attained the maximum (rad s^{-1}) value. Inhibition efficiency was calculated using polarization resistance (R_p) rather than charge transfer resistance (R_{ct}), because R_p can be considered as a sum of charge transfer resistance (R_{ct}), accumulation resistance (R_a), diffusion layer resistance (R_{dl}), film resistance (R_f) etc. [76–79]. The increased values of R_p indicated the adsorption of inhibitor molecules on metallic surface, whereas decreased values of the C_{dl} (Table 6) suggested increase in the thickness of the electric double layer or decrease in value of dielectric constant or a combination of both [54,55,77–79].

Table 6
EIS parameters for mild steel in 1 M HCl in the absence and presence of optimum concentration of AMPs.

Inhibitor	Conc (mM)	R_s	R_p	n	C_{dl}	$\eta\%$
Blank	...	0.58	10.7	0.827	106.21	–
AMP-1	0.362	0.935	156.8	0.842	26.42	93.17
AMP-2	0.362	0.933	209.4	0.854	29.40	94.89
AMP-3	0.362	0.842	227.4	0.865	22.20	95.29
AMP-4	0.362	0.966	265.9	0.886	21.06	95.97

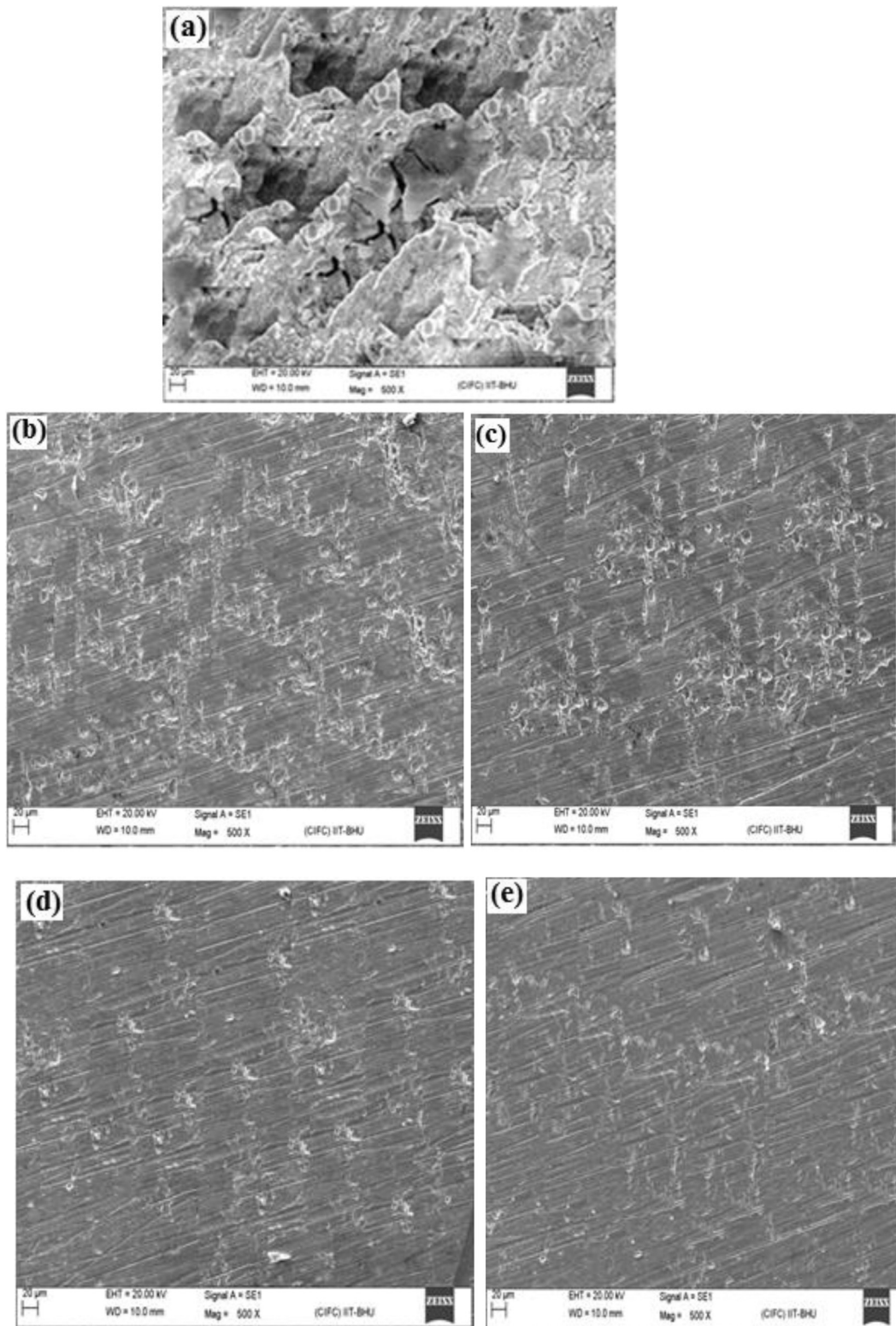


Fig. 6. SEM images of mild steel surfaces in 1 M HCl in the (a) absence of AMPs, and presence of optimum concentration of (b) AMP-1, (c) AMP-2, (d) AMP-3, and (e) AMP-4.

Surface analyses

Scanning electron microscopy

In order to support the suggestions from weight loss and electrochemical studies that AMPs inhibit mild steel corrosion in 1 M HCl by adsorbing on metallic surface, scanning electron microscopic (SEM) study was carried out to analyze the surface of the

steel immersed in 1 M HCl in the absence and presence of optimum concentration of the inhibitors. Fig. 6 represents the SEM images recorded for mild steel surface after immersion in the aggressive acid solution which causes destructive attack on the metallic surface in absence of the inhibitors (Fig. 6a). Mild steel surface was seriously corroded in the acid solution without the inhibitor molecules, leading to highly damaged surface characterized with moun-

tain like appearances, pits and cracks as shown in Fig. 6a. This is because the corrosion process was uninhibited and occurred at relatively high rate.

However, in the presence of optimum concentration of AMPs (Fig. 6b–e), the surface morphology of the specimens are relatively smoother owing to the formation of protective film on the steel surface by inhibitor molecules, perhaps through adsorption. Careful inspection and qualitative interpretation of the SEM images in presence of inhibitor molecules suggest that the order of surface smoothness for the AMPs is in the order: AMP-1 < AMP-2 < AMP-3 < AMP-4, which is in agreement with the order of inhibition efficiency obtained from weight loss and electrochemical studies.

Atomic force microscopy

Additional proof of adsorption of inhibitor molecules on mild steel surface was provided using AFM machine. Just like in the case of SEM, the analysis was performed for mild steel surface in 1 M HCl in the absence and presence of optimum concentration of AMPs. Three dimensional AFM micrographs obtained for inhibited and uninhibited mild steel specimens are shown in Fig. 7. It can be seen from Fig. 7a that the AFM micrograph of the steel surface in

the absence of inhibitors showed highly damaged and corroded surface, which is due to unhindered acid corrosion of the metallic surface. The calculated average surface roughness for uninhibited corroding specimen was 396 nm. However, the AFM images in the presence of the inhibitors (Fig. 7b–e) showed significantly reduced surface roughnesses; the surface is smoother, suggesting a subdued corrosive attack. The calculated average surface roughness values were 265, 184, 167, 139 nm for mild steel specimens in 1 M HCl in the presence of optimum concentration of AMP-1, AMP-2, AMP-3 and AMP-4, respectively. Increased surface smoothness in the presence of the inhibitors is attributed to the formation of adsorbed protective film of the inhibitor molecules, which separates the metal from aggressive acid solution, thereby inhibiting mild steel corrosion.

Computational studies

Quantum chemical calculations

The optimized, HOMO and LUMO molecular structures of neutral gas phase (AMPs-Gas), neutral solvated (AMPs-Sol) and protonated (AMPs-H⁺) of AMP molecules are shown in Figs. 8 and 9.

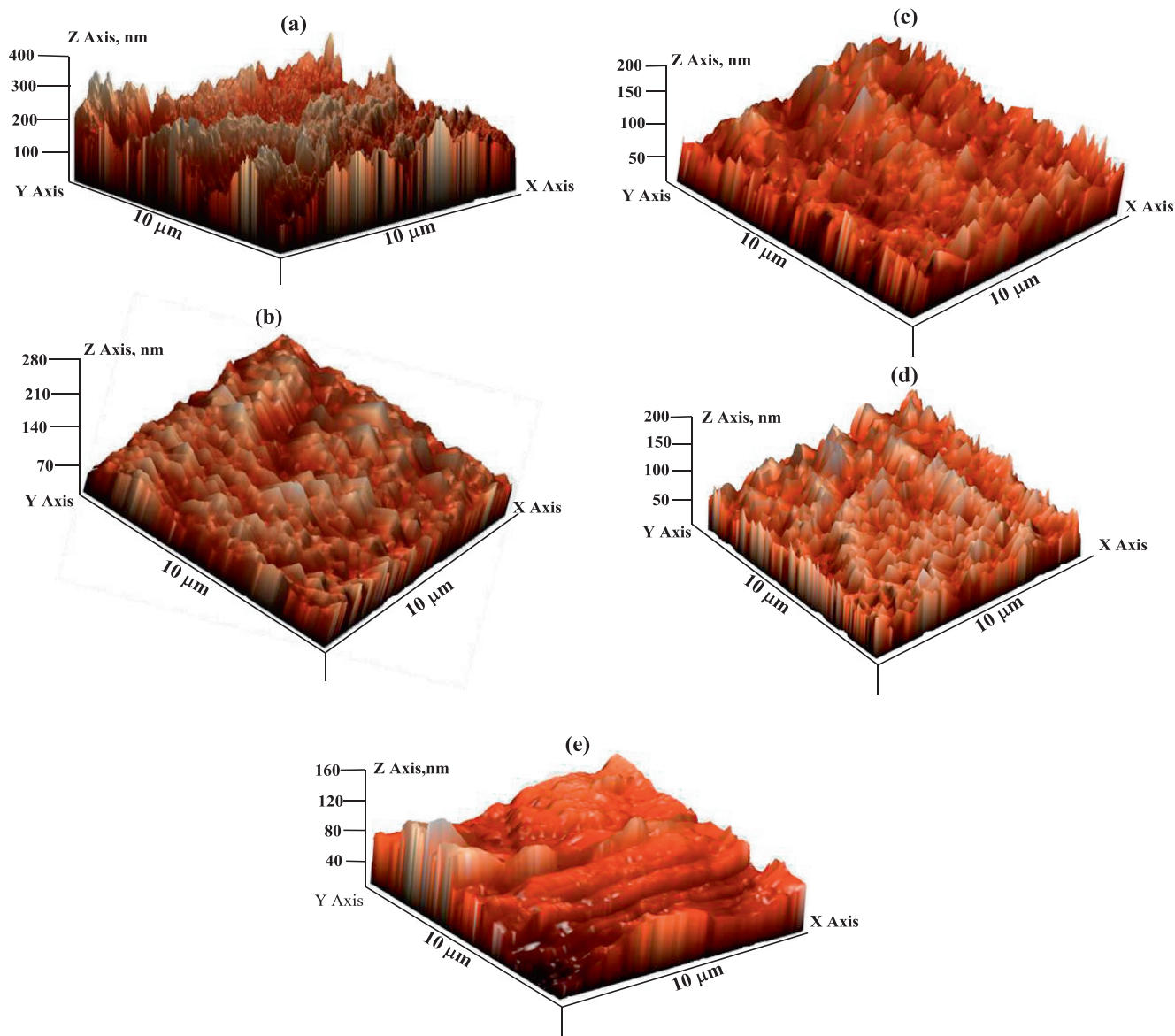


Fig. 7. AFM images of mild steel surfaces in 1 M HCl in the (a) absence of AMPs, and presence of optimum concentration of (b) AMP-1, (c) AMP-2, (d) AMP-3, and (e) AMP-4.

Obviously, organic compounds exist in their solvated phase in aqueous acidic medium like 1 M HCl therefore the DFT study have also been carried out in the solvation phase. More so, the heteroatoms such as N, S and O can also undergo protonation in highly acidic medium of 1 M HCl therefore the DFT study has also been carried out for the protonated form of the AMP molecules. The most stable conformation for each AMP molecule corresponds to the geometry that affords H-bonding between the H-atom of the phenylamino moiety and the 6-carbonyl oxygen of the pyrimidinetrione. The most stable structures of the molecules are nearly planar. This might contribute to good corrosion inhibition performances, because high planarity has been reported to favor optimum adsorption of inhibitor molecules on metallic surface [80–82]. Electron density distributions of HOMO and LUMO are shown in Fig. 9. Both the HOMO and LUMO electron densities are essentially delocalized over the molecules such that nearly all the atoms are involved. This suggests that a large fractions of the molecular orbitals of AMPs can actively interact with metallic orbitals either via electron donation to the appropriate orbitals of the metal or electron acceptance from suitable occupied metallic orbitals.

The local sites of reactivity in AMP molecules were observed using the Fukui indices. The electron density isosurfaces for nucleophilic (f_k^+) and electrophilic (f_k^-) Fukui functions for neutral gas phase form of AMP molecules are shown in Fig. 10. Atomic sites with high values of f_k^+ are said to be highly susceptible to nucleophilic attacks, while those with substantial values of f_k^- are more prominent to electrophilic attacks. A corroding mild steel surface in acidic medium is bound to be positively charged, or sometimes

have a layer of negatively charged acid anions on the positively charged surface [43]. The steel surface may therefore be either nucleophilic or electrophilic, having affinity to interact with appropriate sites in the inhibitor molecule. As shown in Fig. 10, the O-atoms of the tricarbonyl functional groups in pyrimidinetrione exhibit propensities for both nucleophilic and electrophilic attacks, having considerable electron densities for both f_k^+ and f_k^- . The methylene group adjoining phenylamino and pyrimidinetrione moieties is a potential site for nucleophilic attack in all the AMPs. The $-\text{NO}_2$ substituent group in AMP-1 is also susceptible to nucleophilic attack. The N-atoms of the pyrimidine ring are less disposed to attacks by electron-rich specie. In all the AMP molecules, the N-atom of phenylamino sub-structure is a prominent site for electrophilic attacks. The $-\text{OH}$ groups in AMP-3 and AMP-4 are also predisposed to attacks by electron-deficient specie.

Values of some quantum chemical descriptors of the studied AMP molecules for their neutral gas, neutral solvated and protonated forms are listed in Table 7. The FMO energy parameters are popularly used to describe the tendency of an inhibitor molecule to donate or accept electrons in appropriate situations. A molecule with higher value of E_{HOMO} is generally considered to have higher tendency to donate its HOMO electrons to suitable vacant metallic orbitals. On the other hand, a molecule with lower value of E_{LUMO} is basically expected to display better penchant for electron acceptance into its LUMO orbital from appropriate occupied orbitals of the metal [42,43,80,81]. The trend of E_{HOMO} values for the AMPs is AMP-4 > AMP-3 > AMP-2 > AMP-1, which corresponds to the order of observed inhibition efficiencies. The results

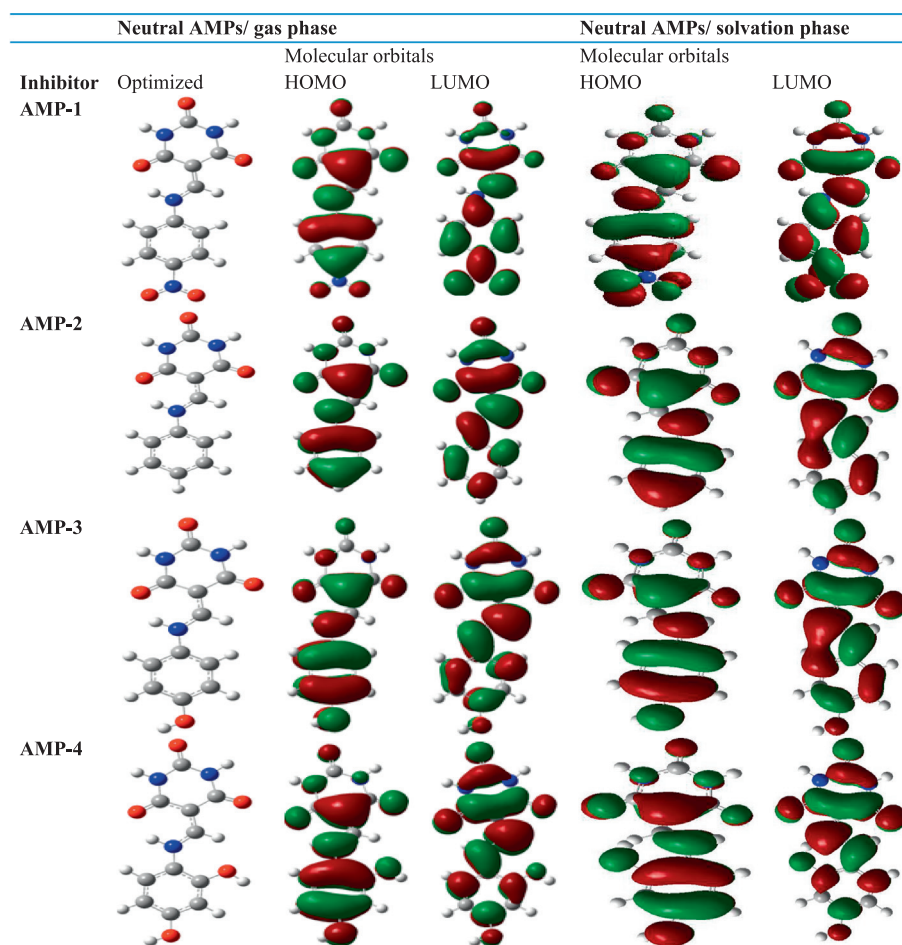


Fig. 8. Optimized, HOMO and LUMO frontier molecular orbital pictures of AMP molecules in neutral gas phase and solvated phase.

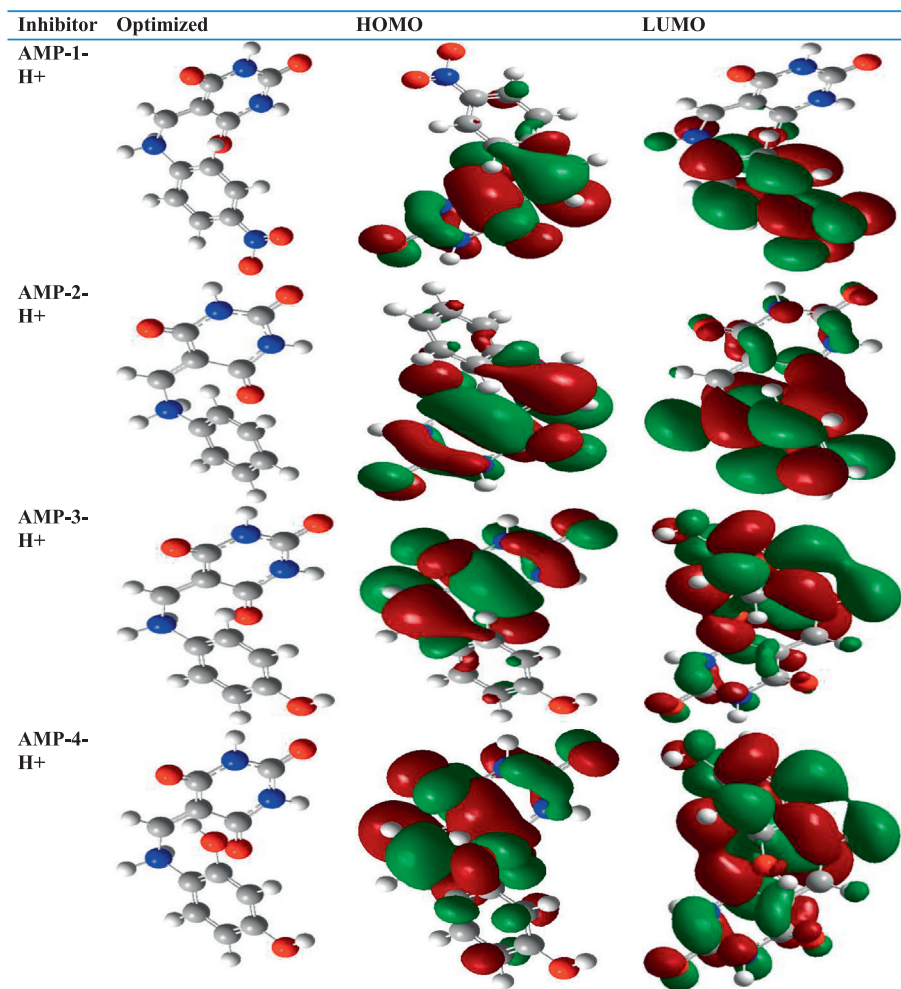


Fig. 9. Optimized, HOMO and LUMO frontier molecular orbital pictures of protonated form of AMP molecules.

of E_{LUMO} and energy gap (ΔE) do not provide such direct correlation with the experimental inhibition strengths.

A molecule with small value of χ is considered to have relatively weak tendency of retaining its own electrons during donor–acceptor interactions. Such molecule has better tendency of donating its electrons to a nearby electrophilic species. The order of electronegativity of the studied molecules is AMP-4 < AMP-3 < AMP-2 < AMP-1, which agrees with the experimentally derived order of decreasing inhibition efficiencies of the molecules (from AMP-4 to AMP-1). The magnitudes of ΔN in Table 7 suggest that the inhibition efficiencies of AMPs increase with increasing electron-donating ability [82] of the molecules. The decreasing order of ΔN is AMP-4 > AMP-3 > AMP-2 > AMP-1, which is in agreement with the trend of experimental inhibition efficiencies. In other words, AMP-4 with highest fraction of electrons transferred to the metal has the highest corrosion inhibition potential. Large dipole moment has been reported to favour high corrosion inhibition efficiency by enhancing dipole–dipole interactions between the inhibitor molecules and the metal surface [42,83]. The dipole moments of AMPs are in the order AMP-4 > AMP-3 > AMP-2 > AMP-1, which again corroborates the observed trend of experimental inhibition efficiencies. The DFT parameters derived for solvated and protonated forms of AMP molecules are almost constant with those derived for neutral gas phase of the AMP molecules. It is important to note that most of the DFT indices are constant with the trend of experimental protection ability of AMP molecules, however, some of the DFT indices showed irregular

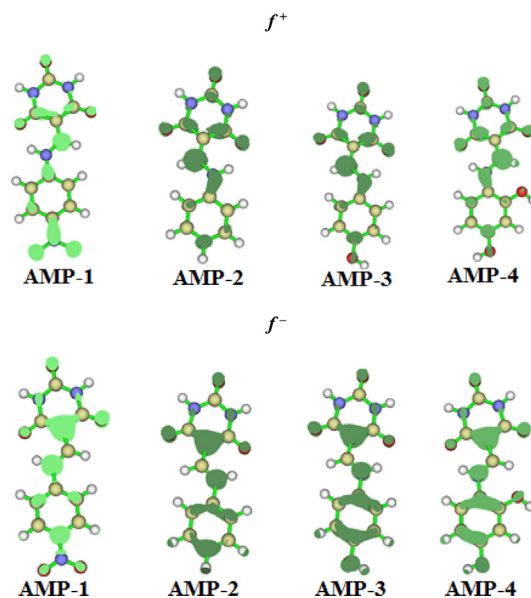


Fig. 10. Nucleophilic (f^+) and electrophilic (f^-) Fukui indices of AMPs visualized at 0.003 electron density isosurface.

trends. For solvated and protonated forms of AMP molecules, the values of E_{HOMO} are increasing on going AMP-1 to AMP-4 which is according to the trend of observed inhibition efficiencies of these

Table 7
Selected quantum chemical parameters for AMP-1, AMP-2, AMP-3 and AMP-4 in their neutral gas phase (AMPs-Gas), aqueous phase (AMPs-Sol) and protonated forms (AMPs-H⁺).

Parameters→ Compounds↓	E _{HOMO} (eV)	E _{LUMO} (eV)	ΔE (eV)	χ (eV)	ΔN	Dipole moment
AMP-1-Gas	-7.183	-3.400	3.783	5.292	0.203	1.743
AMP-2-Gas	-6.600	-2.450	4.151	4.525	0.001	5.293
AMP-3-Gas	-6.296	-2.325	3.970	4.311	0.052	6.225
AMP-4-Gas	-6.133	-2.082	4.051	4.108	0.101	7.567
AMP-1-Sol	-6.387	-2.419	3.963	4.401	0.030	3.670
AMP-2-Sol	-5.817	-1.523	4.293	3.670	0.198	3.016
AMP-3-Sol	-5.368	-1.699	3.668	3.534	0.269	3.336
AMP-4-Sol	-5.430	-1.456	3.973	3.442	0.271	2.815
AMP-1-H ⁺	-6.030	-2.952	3.078	4.491	0.009	8.268
AMP-2-H ⁺	-6.316	-1.363	4.953	3.839	0.137	7.799
AMP-3-H ⁺	-4.548	-0.310	4.237	2.429	0.493	6.472
AMP-4-H ⁺	-3.655	-0.461	3.193	2.058	0.771	6.532

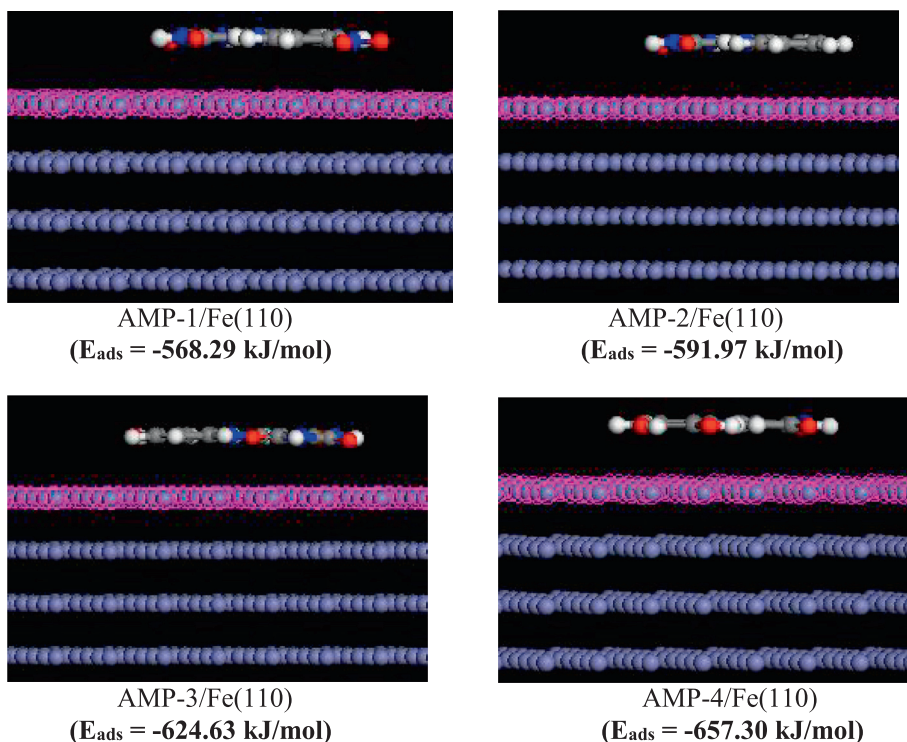


Fig. 11. Equilibrium configurations of AMPs adsorbed on Fe(1 1 0) surface and the corresponding adsorption energies.

inhibitor molecules. Although, the E_{LUMO} values show irregular trends, however the ΔE values for AMPs except at some selected cases well established the experimental trend of observed inhibition efficiency. The values of electronegativities for tested organic inhibitors molecules are accordance to the expectation particularly for protonated form of AMP molecules. Similarly, as expected the ΔN values are increasing from going AMP-1 to AMP-4. In summary, it can be concluded that DFT parameters derived for neutral gas phase, neutral solvated phase and protonated forms of AMP molecules are well consistent with their order of experimental inhibition efficiencies.

Monte Carlo simulations

The equilibrium configurations of AMPs/Fe(1 1 0) are shown in Fig. 11. The results revealed that the inhibitor molecules can approach the steel surface in a flat orientation. The adsorption energy (E_{ads}) is a measure of the strength of interactions between the adsorbate and adsorbent. The more negative the energy, the stronger the adsorption. The order of the magnitudes of E_{ads} values

for AMPs/Fe(1 1 0) (listed in Fig. 11) is AMP-4/Fe(1 1 0) > AMP-3/Fe(1 1 0) > AMP-2/Fe(1 1 0) > AMP-1/Fe(1 1 0), which is in agreement with the observed trend of inhibition efficiencies of the molecules.

Conclusions

Based on the results obtained from experimental and computational studies on the potentials of the newly synthesized 5-arylamino-methylenepyrimidine 2, 4, 6-trione (AMPs) to inhibit mild steel corrosion in 1 M HCl, it can be concluded that the compounds act as efficient inhibitors for mild steel corrosion in 1 M HCl medium. The inhibition efficiency increases with increasing concentration of the inhibitors and the inhibitive strength follows the order: AMP-4 > AMP-3 > AMP-2 > AMP-1. Adsorption of these compounds on mild steel surface obeyed the Temkin adsorption isotherm. Electrochemical impedance spectroscopic (EIS) measurements revealed that the studied AMPs inhibit steel corrosion by adsorbing on the metal/electrolyte interface. Potentiodynamic polarization study revealed that studied compounds act as catho-

dic type inhibitors. SEM and AFM results supported the formation of protective film by inhibitors on the mild steel surface. Quantum chemical calculations suggested that the inhibitive properties of the molecules can be related to their relative ability to donate electrons to metallic orbitals. The presence of electron donating substituent (–OH) in AMP-3 and AMP-4 therefore support their higher inhibition efficiencies compared to the unsubstituted AMP-2 and –NO₂ (electron withdrawing) substituted AMP-1. The predicted adsorption energies for the interactions of AMPs with Fe(1 1 0) crystal surface also agreed with the experimentally observed trend of inhibition potentials.

Acknowledgements

CV and LOO thank the North-West University for granting them Post-Doctoral fellowship.

Appendix A. Supplementary data

Supplementary data associated with this article can be found, in the online version, at <https://doi.org/10.1016/j.rinp.2018.01.008>.

References

- Zhang K, Xu B, Yang W, Yin X, Liu Y, Chen Y. Halogen-substituted imidazole derivatives as corrosion inhibitors for mild steel in hydrochloric acid solution. *Corros Sci* 2015;90:284–95.
- Shaban SM, Aiad I, El-Sukkary MM, Soliman EA, El-Awady MY. Inhibition of mild steel corrosion in acidic medium by vanillin cationic surfactants. *J Mol Liq* 2015;203:20–8.
- Yousefi A, Javadian S, Dalir N, Kakemam J, Akbari J. Imidazolium-based ionic liquids as modulators of corrosion inhibition of SDS on mild steel in hydrochloric acid solutions: experimental and theoretical studies. *RSC Adv* 2015;5:11697–713.
- Lebrini M, Traisnel M, Lagrene M, Mernari B, Bentiss F. Inhibitive properties, adsorption and a theoretical study of 3,5-bis(n-pyridyl)-4-amino-1,2,4-triazoles as corrosion inhibitors for mild steel in perchloric acid. *Corros Sci* 2008;50:473–9.
- Murulana LC, Singh AK, Shukla SK, Kabanda MM, Ebenso EE. Experimental and quantum chemical studies of some Bis(trifluoromethyl-sulfonyl) imide imidazolium-based ionic liquids as corrosion inhibitors for mild steel in hydrochloric acid solution. *Ind Eng Chem Res* 2012;51:13282–99.
- Murulana LC, Kabanda MM, Ebenso EE. Experimental and theoretical studies on the corrosion inhibition of mild steel by some sulphonamides in aqueous HCl. *RSC Adv* 2015;5:28743–61.
- Pandey A, Singh B, Verma C, Ebenso EE. Synthesis, characterization and corrosion inhibition potential of two novel Schiff bases on mild steel in acidic medium. *RSC Adv* 2017;7:47149–63.
- Hasanov R, Bilge S, Bilgiç S, Gece G, Kılıç Z. Experimental and theoretical calculations on corrosion inhibition of steel in 1M H₂SO₄ by crown type polyethers. *Corros Sci* 2010;52:984–90.
- Verma C, Singh P, Bahadur I, Ebenso EE, Quraishi MA. Electrochemical, thermodynamic, surface and theoretical investigation of 2-aminobenzene-1,3-dicarbonitriles as green corrosion inhibitor for aluminum in 0.5M NaOH. *J Mol Liq* 2015;209:767–78.
- Tang Y, Yang X, Yang W, Chen Y, Wan R. Experimental and molecular dynamics studies on corrosion inhibition of mild steel by 2-amino-5-phenyl-1,3,4-thiadiazole. *Corros Sci* 2010;52:242–9.
- Ya R, Levina Velichko FK. Advances in the chemistry of barbituric acids. *Usp Khim* 1960;29:929.
- Ma L, Li S, Zheng H, Chen J, Lin L, Ye X, et al. Synthesis and biological activity of novel barbituric and thiobarbituric acid derivatives against non-alcoholic fatty liver disease. *Euro J Med Chem* 2011;46:2003–10.
- Hello KM, Shneine JK, Numan AA. synthesis and biological activity of some barbituric acid derivatives via Schiff's bases. *Iraqi J Sci* 2009;50:423–30.
- Borjarski JT, Mokros JL, Barton HJ, Paluchowska MH. Recent progress in barbituric acid chemistry. *Adv Heterocyc Chem* 1985;38:229–97.
- Cheng X, Tanaka K, Yoneda F. Simple new method for the synthesis of 5-deaza-10-oxaflavin, a potential organic oxidant. *Chem Pharm Bull* 1990;38:307–11.
- Naguib FNM, Levesque DL, Wang EC, Panzica RP, Kouni, El. MH. 5-Benzylbarbituric acid derivatives, potent and specific inhibitors of uridine phosphorylase. *Biochem Pharmacol* 1993;46:1273–83.
- Grams F, Brandstetter H, D'Alo S. Pyrimidine-2, 4, 6-triones: a new effective and selective class of matrix metalloproteinase inhibitors. *Biol Chem* 2001;382:1277–85.
- Udhayakala PT, Rajendiran V, Gunasekaran S. A theoretical study of some barbiturates as corrosion inhibitors for mild steel. *J Chem Pharm Res* 2014;6:1027–39.
- Özcana M, Solmaz R, Kardas G, Dehri I. Adsorption properties of barbiturates as green corrosion inhibitors on mild steel in phosphoric acid. *Colloids Surf A Physicochem Eng Asp* 2008;325:57–63.
- Quraishi MA, Ansari KR, Yadav DK, Ebenso EE. Corrosion inhibition and adsorption studies of some barbiturates on mild steel/acid interface. *Int J Electrochem Sci* 2012;7:12301–15.
- Hmamou B, Salghi R, Zarrouk A, Aouad MR, Benali O, Zarrok H, et al. Weight loss, electrochemical, quantum chemical calculation, and molecular dynamics simulation studies on 2-(Benzylthio)-1,4,5-triphenyl-1H-imidazole as an inhibitor for carbon steel corrosion in hydrochloric acid. *Ind Eng Chem Res* 2013;52:14315–27.
- de Souza FS, Spinelli A. Caffeic acid as a green corrosion inhibitor for mild steel. *Corros Sci* 2009;51:642–9.
- Eddy NO, Ebenso EE. Adsorption and inhibitive properties of ethanol extract of *Musa sapientum* peels as a green corrosion inhibitor for mild steel in H₂SO₄. *Afr J Pure Appl Chem* 2008;2:46–54.
- Abiola OK, Otaigbe JOE, Kio OJ. *Gossypium hirsutum* L. extracts as green corrosion inhibitor for aluminum in NaOH solution. *Corros Sci* 2009;51:1879–81.
- Beattie C, North M, Villuendas P. Proline-catalysed amination reactions in cyclic carbonate solvents. *Molecules* 2011;16:3420–32.
- Domling A. Recent developments in isocyanide based multicomponent reactions in applied chemistry. *Chem Rev* 2006;106:17–89.
- Singh MS, Chowdhury S. Recent developments in solvent-free multicomponent reactions: a perfect synergy for eco-compatible organic synthesis. *RSC Adv* 2012;2:4547–92.
- Cioc RC, Ruijter E, Orru RVA. Multicomponent reactions: advanced tools for sustainable organic synthesis. *Green Chem* 2014;16:2958–75.
- Sheldon RA. Green solvents for sustainable organic synthesis: state of the art. *Green Chem* 2005;7:267–78.
- Simon MO, Li CJ. Green chemistry oriented organic synthesis in water. *Chem Soc Rev* 2012;41:1415–27.
- Leong WWY, Chen X, Chi YR. NHC-catalyzed reactions of enals with water as a solvent. *Green Chem* 2013;15:1505–8.
- Capello C, Fischer U, Hungerbühler K. What is a green solvent? A comprehensive framework for the environmental assessment of solvents. *Green Chem* 2007;9:927–34.
- Sharghi H, Khalifeh R, Doroodmand MM. Copper Nanoparticles on Charcoal for Multicomponent Catalytic Synthesis of 1,2,3-Triazole Derivatives from Benzyl Halides or Alkyl Halides, Terminal Alkynes and Sodium Azide in Water as a "Green" Solvent. *Adv Synth Catal* 2009;351:207–18.
- Bose DS, Fatima L, Mereyala HB. Green chemistry approaches to the synthesis of 5-Alkoxy carbonyl-4-aryl-3,4-dihydropyrimidin-2(1H)-ones by a three-component coupling of one-pot condensation reaction: comparison of ethanol, water, and solvent-free conditions. *J Org Chem* 2003;68:587–90.
- Dhorajiya BD, Dholakiya BZ. Green chemistry multicomponent protocol for formylation and Knoevenagel condensation for synthesis of (Z)-5-arylaminoethylene pyrimidine 2, 4, 6-trione derivatives in water BDDDBZ Dholakiya. *Green Chem Lett Rev* 2014;7:1–10.
- Verma C, Quraishi MA, Ebenso EE. Mannich bases derived from melamine, formaldehyde alkanoleamines as novel corrosion inhibitors for mild steel in hydrochloric acid medium. *Int J Electrochem Sci* 2013;8:10851–63.
- Verma C, Quraishi MA, Singh A. 2-Amino-5-nitro-4,6-diaryl cyclohex-1-ene-1,3,3-tricarbonitriles as new and effective corrosion inhibitors for mild steel in 1M HCl: Experimental and theoretical studies. *J Mol Liq* 2015;212:804–12.
- Frisch MJ, Trucks GW, Schlegel HB, Scuseria GE, Robb MA, Cheeseman JR, et al. *Gaussian 09, Revision D.01*; Gaussian, Inc.: Wallingford CT, 2009.
- Becke AD. Density-functional thermochemistry. III. The role of exact exchange. *J Chem Phys* 1993;98:5648–52.
- Becke AD. Density-functional exchange-energy approximation with correct asymptotic behavior. *Phys Rev A* 1988;38:3098–100.
- Lee C, Yang W, Parr RG. Development of the Colle-Salvetti correlation-energy formula into a functional of the electron density. *Phys Rev B* 1988;37:785–9.
- Olasunkanmi LO, Obot IB, Kabanda MM, Ebenso EE. Some quinoxalin-6-yl derivatives as corrosion inhibitors for mild steel in hydrochloric acid: experimental and theoretical studies. *J Phys Chem C* 2015;119:16004–19.
- Olasunkanmi LO, Kabanda MM, Ebenso EE. Quinoxaline derivatives as corrosion inhibitors for mild steel in hydrochloric acid medium: electrochemical and quantum chemical studies. *Physica E* 2016;76:109–26.
- Martinez S. Inhibitory mechanism of mimosa tannin using molecular modeling and substitutional adsorption isotherms. *Mater Chem Phys* 2003;77:97–102.
- Pearson RG. Absolute electronegativity and hardness: application to inorganic chemistry. *Inorg Chem* 1988;27:734–40.
- Gomez B, Likhanova NV, Dominguez MA, Martinez-Palou R, Vela A, Gazquez JL. Quantum chemical study of the inhibitive properties of 2-Pyridyl-Azoles. *J Phys Chem B* 2006;110:8928–34.
- Yan Y, Wang X, Zhang Y, Wang P, Zhang J. Theoretical evaluation of inhibition performance of purine corrosion inhibitors. *Mol Sim* 2013;39:1034–41.
- Yang W, Mortier WJ. The use of global and local molecular parameters for the analysis of the gas-phase basicity of amines. *J Am Chem Soc* 1986;108:5708–11.
- Lu T, Chen F. Multiwfn: a multifunctional wavefunction analyzer. *J Comp Chem* 2012;33:580–92.
- Lu T, Chen F. Quantitative analysis of molecular surface based on improved Marching Tetrahedra algorithm. *J Mol Graph Model* 2012;38:314–23.

- [51] Verma C, Ebenso EE, Bahadur I, Obot IB, Quraishi MA. 5-(Phenylthio)-3H-pyrrole-4-carbonitriles as effective corrosion inhibitors for mild steel in 1M HCl: Experimental and theoretical investigation. *J Mol Liq* 2015;212:209–18.
- [52] Verma C, Quraishi MA, Olasunkanmi LO, Ebenso EE. L-Proline-promoted synthesis of 2-amino-4-arylquinoline-3-carbonitriles as sustainable corrosion inhibitors for mild steel in 1 M HCl: experimental and computational studies. *RSC Adv* 2015;5:85417–30.
- [53] Verma C, Olasunkanmi LO, Obot IB, Ebenso EE, Quraishi MA. 5-Arylpyrimido-[4,5-b]quinoline-diones as new and sustainable corrosion inhibitors for mild steel in 1 M HCl: a combined experimental and theoretical approach. *RSC Adv* 2016;6:15639–54.
- [54] Verma C, Quraishi MA, Singh A. 2-Aminobenzene-1,3-dicarbonitriles as green corrosion inhibitors for mild steel in 1M HCl: Electrochemical, thermodynamic, surface and quantum chemical investigation. *J Taiwan Inst Chem Eng* 2015;49:229–39.
- [55] Verma C, Quraishi MA, Singh A. A thermodynamical, electrochemical, theoretical and surface investigation of diheteroaryl thioethers as effective corrosion inhibitors for mild steel in 1 M HCl. *J Taiwan Inst Chem Eng* 2016;58:127–40.
- [56] Verma C, Singh A, Pallikonda G, Chakravarty M, Quraishi MA, Bahadur I, Ebenso EE. Aryl sulfonamidomethylphosphonates as new class of green corrosion inhibitors for mild steel in 1M HCl: electrochemical, surface and quantum chemical investigation. *J Mol Liq* 2015;209:306–19.
- [57] Bai L, Feng LJ, Wang HY, Lu YB, Lei XW, Bai FL. Comparison of the synergistic effect of counterions on the inhibition of mild steel corrosion in acid solution: electrochemical, gravimetric and thermodynamic studies. *RSC Adv* 2015;5:4716–26.
- [58] Wadhvani PM, Ladha DG, Panchal VK, Shah NK. Enhanced corrosion inhibitive effect of p-methoxybenzylidene-4,4'-dimorpholine assembled on nickel oxide nanoparticles for mild steel in acid medium. *RSC Adv* 2015;5:7098–111.
- [59] Gupta NK, Verma C, Salghi R, Lgaz H, Mukherjee AK, Quraishi MA. New phosphonate based corrosion inhibitors for mild steel in hydrochloric acid useful for industrial pickling processes: experimental and theoretical approach. *New J Chem* 2017;41:13114–29.
- [60] Haque J, Srivastava V, Verma C, Lgaz H, Salghi R, Quraishi MA. N-Methyl-N, N-trioctylammonium chloride as a novel and green corrosion inhibitor for mild steel in an acid chloride medium: electrochemical, DFT and MD studies. *New J Chem* 2017. <https://doi.org/10.1039/C7NJ02254A>.
- [61] Verma CB, Quraishi MA, Ebenso EE. Electrochemical and Thermodynamic Investigation of Some Soluble Terpolymers as effective corrosion inhibitors for Mild Steel in 1M hydrochloric acid solution. *Int J Electrochem Sci* 2013;8:12894–906.
- [62] Verma C, Singh P, Quraishi MA. Journal of the association of arab universities for basic and applied sciences. *J Assoc Arab Univ Basic Appl Sci* 2016;21:24–30.
- [63] Schmid GM, Huang HJ. Spectro-electrochemical studies of the inhibition effect of 4, 7-diphenyl -1, 10-phenanthroline on the corrosion of 304 stainless steel. *Corros Sci* 1980;20:1041–57.
- [64] Ashassi-Sorkhabi H, Shaabani B, Seifzadeh D. Corrosion inhibition of mild steel by some schiff base compounds in hydrochloric acid. *Appl Surf Sci* 2005;239:154–64.
- [65] Umoren SA, Eduok UM, Oguzie EE. Corrosion inhibition of mild steel in 1 M H₂SO₄ by polyvinyl pyrrolidone and synergistic iodide additives. *Portugaliae Electrochimica Acta* 2008;26:533–46.
- [66] Albrimi YA, Addi AA, Douch J, Souto RM, Hamdani M. Inhibition of the pitting corrosion of 304 stainless steel in 0.5M hydrochloric acid solution by heptamolybdate ions. *Corros Sci* 2015;90:522–8.
- [67] Goulart CM, Esteves-Souza A, Martinez-Huitle CA, Rodrigues CJF, Maciel MAM, Echevarria A. Experimental and theoretical evaluation of semicarbazones and thiosemicarbazones as organic corrosion inhibitors. *Corros Sci* 2013;67:281–91.
- [68] Amin MA, Ibrahim MM. Corrosion and corrosion control of mild steel in concentrated H₂SO₄ solutions by a newly synthesized glycine derivative. *Corros Sci* 2011;53:873–85.
- [69] Issaadi S, Douadi T, Zouaoui A, Chafaa S, Khan MA, Bouet G. Novel thiophene symmetrical Schiff base compounds as corrosion inhibitor for mild steel in acidic media. *Corros Sci* 2011;53:1484–8.
- [70] Amin MA, Ahmed MA, Arida HA, Arslan T, Saraçoglu M, Kandemirli F. Monitoring corrosion and corrosion control of iron in HCl by non-ionic surfactants of the TRITON-X series – Part II. Temperature effect, activation energies and thermodynamics of adsorption. *Corros Sci* 2011;53:540–8.
- [71] Yıldız R, Dogan T, Dehri I. Evaluation of corrosion inhibition of mild steel in 0.1M HCl by 4-amino-3-hydroxynaphthalene-1-sulphonic acid. *Corros Sci* 2014;85:215–21.
- [72] Solmaz R. Investigation of corrosion inhibition mechanism and stability of Vitamin B1 on mild steel in 0.5M HCl solution. *Corros Sci* 2014;81:75–84.
- [73] Xu B, Ji Y, Zhang X, Jin X, Yang W, Chen Y. Experimental and theoretical studies on the corrosion inhibition performance of 4-amino-N, N-di-(2-pyridylmethyl)-aniline on mild steel in hydrochloric acid. *RSC Adv* 2015;5:56049–59.
- [74] Chevalier M, Robert F, Amusan N, Traisnel M, Roos C, Lebrini M. Enhanced corrosion resistance of mild steel in 1M hydrochloric acid solution by alkaloids extract from Aniba rosaedora plant: Electrochemical, phytochemical and XPS studies. *Electrochimica Acta* 2014;131:96–105.
- [75] Ebenso EE, Kabanda MM, Murulana LC, Singh AK, Shukla SK. Electrochemical and quantum chemical investigation of some azine and thiazine dyes as potential corrosion inhibitors for mild steel in hydrochloric acid solution. *Ind Eng Chem Res* 2012;51:12940–58.
- [76] Roy P, Karfa P, Adhikari U, Sukul D. Corrosion inhibition of mild steel in acidic medium by polyacrylamide grafted Guar gum with various grafting percentage: Effect of intramolecular synergism. *Corros Sci* 2014;88:246–53.
- [77] Solmaz R, Kardas G, Ulha MC, Yazıcı B, Erbil M. Investigation of adsorption and inhibitive effect of 2-mercaptothiazoline on corrosion of mild steel in hydrochloric acid media. *Electrochimica Acta* 2008;53:5941–52.
- [78] Ozcan M, Dehri I, Erbil M. Organic sulphur-containing compounds as corrosion inhibitors for mild steel in acidic media: correlation between inhibition efficiency and chemical structure. *Appl Surf Sci* 2004;236:155–64.
- [79] Solmaz R. Investigation of the inhibition effect of 5-((E)-4-phenylbuta-1,3-dienylideneamino)-1,3,4-thiadiazole-2-thiol Schiff base on mild steel corrosion in hydrochloric acid. *Corros Sci* 2010;52:3321–30.
- [80] Singh P, Ebenso EE, Olasunkanmi LO, Obot IB, Quraishi MA. Electrochemical, theoretical, and surface morphological studies of corrosion inhibition effect of green naphthyridine derivatives on mild steel in hydrochloric acid. *J Phys Chem C* 2016;120:3408–19.
- [81] Arslan T, Kandemirli F, Ebenso EE, Love I, Alemu H. Quantum chemical studies on the corrosion inhibition of some sulphonamides on mild steel in acidic medium. *Corros Sci* 2009;51:35–47.
- [82] Lukovits I, Kálmán E, Zucchi F. Corrosion inhibitors—correlation between electronic structure and efficiency. *Corrosion* 2001;57:3–8.
- [83] Abdulhadi K, Al-Okbi AK, Jamil DM, Qussay A, Al-Amiery AA, Sumer GT, et al. Experimental and theoretical studies of benzoxazines corrosion inhibitors. *Results Phys* 2017;7:4013–9.